Biophysically-based Simulation of Sun-induced Skin Appearance Changes

Xueyan He[1,*] , Minghao Huang[1,*] , Ruoyu Fu[1] , Jie Guo[1,†] , Junping Yuan[1] , Yanghai Wang[1] and Yanwen Guo[1]

[1]Nanjing University, China

Figure 1: *A scene of a man sunbathing on the beach rendered with our method. The left image depicts the initial state of the skin before sunlight exposure. The middle and right images show the skin after 2 days and 10 days of sunlight exposure, respectively. Only the skin appearance of the legs changes, as the other body parts are coated with sunscreen. Our method clearly presents the trend of the skin turning red (erythema) and then darkening (tanning) after sunlight exposure, providing a realistic result.*

Abstract

Skin appearance modeling plays a crucial role in various fields such as healthcare, cosmetics and entertainment. However, the structure of the skin and its interaction with environmental factors like ultraviolet radiation are very complex and require further detailed modeling. In this paper, we propose a biophysically-based model to illustrate the changes in skin appearance under ultraviolet radiation exposure. It takes ultraviolet doses and specific biophysical parameters as inputs, leading to variations in melanin and blood concentrations, as well as the growth rate of skin cells. These changes bring alteration of light scattering, which is simulated by random walk method, and result in observable erythema and tanning. We showcase effects of various skin tones, comparisons across different body parts, and images illustrating the impact of occlusion. It demonstrates superior quality to the the commonly used method with more convincing skin details and bridges biological insights with visual simulations.

CCS Concepts
• Computing methodologies → Physical simulation;

1. Introduction

Human skin is one of the most common materials encountered in our daily lives. Due to its complex multilayered structure containing spatially varying absorptive and scattering chromophores, human skin typically exhibits intricate subsurface scattering appearances under illumination. Additionally, the interactions of skin with different environmental factors such as light and temporal changes are quite complex and constitutes a crucial research area [IGAJG15, CB19, SLDW22]. For example, ultraviolet (UV) radiation poses a significant challenge for skin, leading to various appearance changes like erythema, tanning, and premature aging [EKPR20]. Therefore, rendering and simulating skin remains a challenging yet valuable research direction in the field of computer graphics. It aids in the diagnosis and treatment of dermatological conditions, contributing to advancements in healthcare. In the cosmetics industry, skin computational simulations play a crucial role

---

in product development, guiding the formulation of cosmetics and protective lotions to enhance skin health and appearance. In entertainment, such simulations are utilized to create lifelike images of human features in movies and games, enriching visual storytelling and gaming experiences.

Numerous computer graphics studies are dedicated to modeling skin-environment interactions, including long-term effects like skin aging [IGAJG15], simulating skin appearance in the high spectral range [CBKM15] and the variations of skin under different geographical latitudes and longitudes [SLDW22]. Notably, Chen et al. introduce a novel framework based on physiological principles to simulate the dynamics of skin tanning [CB19]. While the paper primarily focuses on describing the process of tanning, it overlooks the phenomenon of erythema, which is another common and significant transformation in skin appearance resulting from excessive exposure to UV radiation. Therefore, it is important to consider erythema alongside tanning when studying the effects of UV radiation on the skin. However, despite mathematical links to erythema changes under UV irradiation have been proposed in the field of biology [Dif21, DF17, RPW10], it still has not migrated to the field of graphics for further simulation. Inspired by previous work [CB19], we further analyze the correlation between different skin tones and UV radiation interaction, establishing a biological connection to the temporal changes in skin erythema under UV radiation exposure.

In this paper, we propose a discrete time-stepping model to describe the temporal influence of UV radiation on skin appearance and realize the simulation of erythema and tanning under specific UV doses. We normalize skin color to the CIE color space so as to qualitatively calculate the minimum UV dose required to induce erythema or tanning corresponding to each skin tone. By establishing functions describing the temporal variations of skin biophysical parameters under the given UV radiation exposure, updated skin biophysical parameters are computed. These parameters are then used in an improved biophysically-based skin model to render changes in skin appearance in our rendering pipeline.

In summary, the contributions of our work are as follows:

- A mechanism that describes the time-dependent variations of skin appearance under the given UV radiation exposure.
- A comprehensive model for simulating skin structure while simplifying the computation of attenuation coefficients through iterative distance generation.
- A rendering pipeline showcasing the appearance variations of different skin tones under UV radiation.

The remainder of this paper is organized as follows. We give an overview of related work in Section 2. In Section 3, we describe our method. We then present the results of our research and evaluate the effectiveness of our simulation in Section 4. Finally, we summarize the paper in Section 5.

2. Related work

2.1. Modeling of Skin Appearance

From the perspective of rendering methods, models used for generating realistic skin appearance can be broadly classified into two categories: approximate models and stochastic models.

Approximate models primarily focus on simulating subsurface scattering by pre-computing or approximating the random walk behavior of scattered lights within the medium. One prominent approach is the diffusion profile method [DJ05, Jim12, Chr15], which precomputes the behavior of scattered lights within the medium and utilizes a lookup table for fast querying of results by the bidirectional subsurface scattering reflection distribution function (BSSRDF). These methods are fast, straightforward and suitable for real-time rendering applications. Further advancements include spectral BSSRDF proposed by Donner and Jensen [DJ06], which utilizes biological coefficients to control skin color physiologically.

In contrast to diffusion-based rendering methods, the film industry widely employs stochastic methods, which directly simulate physically accurate light transport to present skin appearance [Han15, KNK*16, WVH17]. These methods, particularly effective at skin edges (e.g., nose and ears) [CKB16], are computationally intensive. Krishnaswamy and Baranoski introduced a biophysical skin spectral model, which uses a volume path tracer to render, ensuring biological accuracy by considering all components of light propagation within skin tissue across five layers [KB04]. Chen et al. proposed the first hyperspectral skin appearance model, simulating both spectral and spatial light distributions interacting with skin across UV, visible and infrared domains [CBKM15].

Both approximate models and stochastic models require establishing mappings between biological parameters (typically hemoglobin concentration, melanin concentration, etc.) and rendering parameters such as absorption and reduced scattering coefficients within the models.

2.2. Modeling of Skin Appearance Changes

Many studies have focused on simulating potential changes in skin appearance under different circumstances. Iglesias et al. introduced a model for age-related changes in skin, reproducing variations in optical properties due to aging, including the slimming of the dermis and epidermis, the flattening of the dermo-epidermal junction as well as changes in the concentration of its main chromophores [IGAJG15]. However, this work employs the diffusion profile method [JB02], which may lack physical accuracy. Jimenez et al. [JSB*10] specifically aim to simulate changes in the appearance of skin under different facial expressions by utilizing dedicated hardware to capture the variations in the skin's biological parameters. The others try to use a deep learning model to simulate facial expressions, decomposing them into melanin, hemoglobin, shading, and specular maps [JKLY23]. Notably, Chen et al. introduce a novel framework based on physiological principles to simulate the dynamics of skin tanning [CB19]. It incorporates first-principles algorithms that accurately model the physiological reactions of cutaneous tissues to spectrally-dependent light stimulation. Nevertheless, it just focuses on the tanning and ignores the erythema induced by UV radiation. In contrast to these methods, we propose a comprehensive discrete time-stepping model that captures various temporal effects of UV radiation on skin appearance. This model not only enables the simulation of tanning transformations under specific UV doses but also allows for the simulation of erythema, which is a commonly experienced cutaneous inflammation in our daily lives.
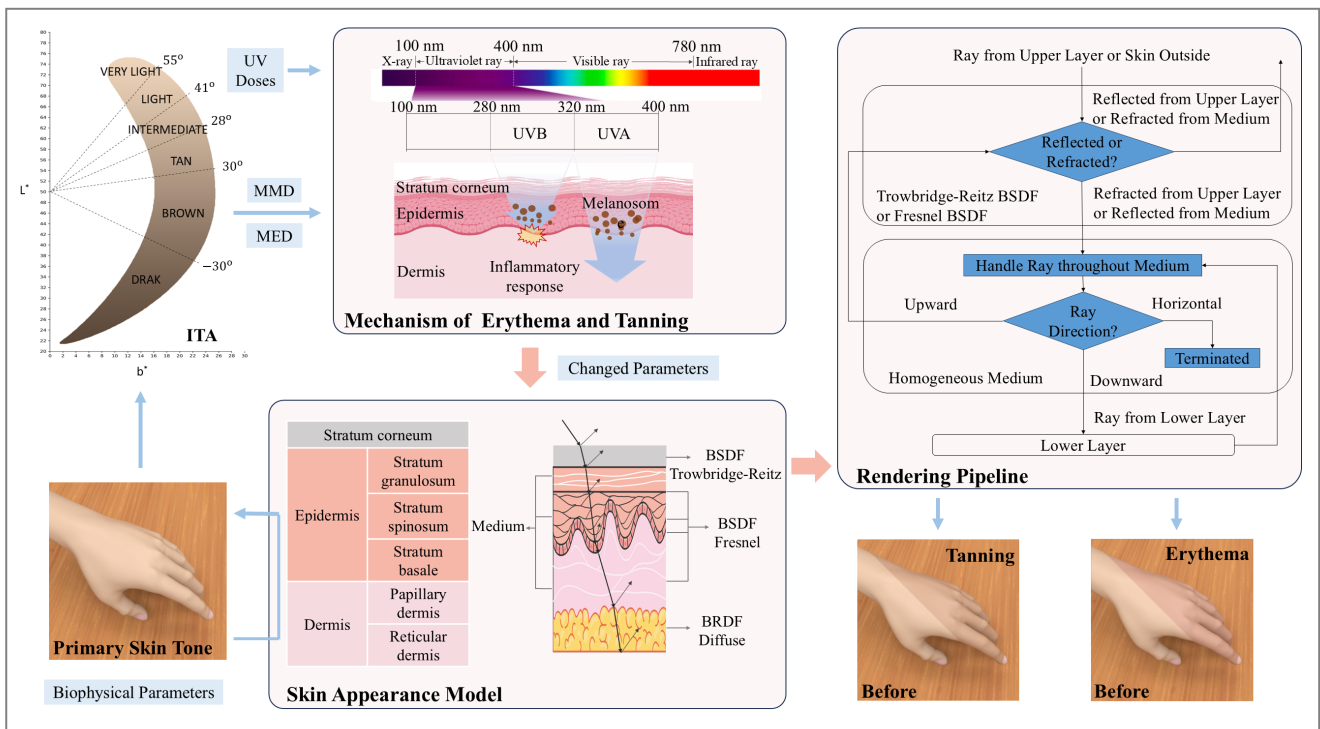
Figure 2: *A flowchart describing our simulation process of skin appearance changes after UV radiation exposure. It is divided into four main parts: ITA-based exposure parameter calculation, erythema and tanning mechanisms, biophysically-based skin appearance model, and the skin rendering pipeline. The inputs are skin biophysical parameters and UV dose, and the output is a simulated image of the skin post-exposure.*

2.3. Skin Changes After UV Radiation Exposure

Exposure to UV radiation triggers both acute inflammatory responses, such as erythema, and adaptive processes collectively known as photoadaptation, which involve melanogenesis and epidermal hyperplasia [LBMZ04]. One of the most noticeable appearance changes after UV radiation exposure is erythema, which results from increased blood volume in the superficial and deep dermal vessels [Dif21]. This acute inflammatory reaction occurs within hours of UV radiation exposure and is accompanied by marked dilation of blood vessels, potentially leading to edema and white blood cell accumulation [AF21]. Epidermal hyperplasia becomes noticeable within 2 days of UV radiation exposure in mice, peaks around a week, and returns to normal within 2 months without further stimulation [Dif21]. This hyperplasia involves an increase in the thickness of the epidermis, which is the outermost layer of the skin. Photoadaptation also involves melanogenesis, which is the production of melanin. Melanin is a potent UV absorber and provides better protection for individuals with darker skin tones compared to those with lighter skin. It acts as a natural defense mechanism against UV radiation by absorbing and scattering it, reducing its penetration to basal epidermal cells [LATdO*97, CB19].

In the traditional understanding, skin redness is typically linked to higher levels of hemoglobin in the local area, while skin pigmentation is primarily associated with melanin. In some studies [BGZ01, SK04], melanin levels noticeably rose by day 7 and remained steady over the following three weeks, mirroring the observed changes in pigmentation (or tanning) as noted clinically. On the other hand, oxyhemoglobin levels spiked within 24 hours, aligning closely with the clinical assessment of erythema (redness), before gradually declining back to baseline levels.

3. Method

Figure 2 provides an overview of the necessary modules and data flow of our method. It utilizes ITA-based UV radiation exposure doses and initial values for specific biophysical parameters of a given skin sample as input. By establishing functions describing temporal variations of skin biophysical parameters under the given UV radiation exposure, updated skin biophysical parameters are computed. These parameters are then used in an improved biophysically-based skin model to render changes in skin appearance, typically erythema and tanning effects. Within these modules, we evaluate the ITA-based UV radiation exposure doses (as discussed in Section 3.1) to determine if they are adequate to induce appearance changes over time, taking into account differences in skin tones. Subsequently, the calculated UV radiation doses are

Symbol	Description
MED	Minimal erythema dose
MMD	Minimal melanin dose
ITA	Individual typology angle, skin color measurement index based on CIE Lab color space
$f(\psi)$	Fraction of maximal skin redness f due to a UV dose input ψ
$R(\Delta t)$	Erythema relative to the maximum redness, $R(t)$, at time Δt
$c(t)$	Blood concentration in the dermis layer at time t
$\hat{m}_i(t)$	Relative melanin content in layer i at time t
$\tau_p(t)$	Production rate of skin cell at time t
$\tau(t)$	Actual thickness at time t

Table 1: *Main symbols used in the paper.*

used to induce erythema and tanning changes in people with different skin tones (as outlined in Section 3.2 and Section 3.3), resulting in adjustments to biophysical parameters. Later, a biophysically-based skin model is introduced in Section 3.4, which is based on the work of Chen et al. [CBKM15]. To achieve the final appearance changes of the skin, a rendering pipeline based on random walk method is introduced in Section 3.5. Here we introduce the main symbols used in our study, as shown in Table 1.

3.1. UV Dose Calculation

The skin's adaptation to UV radiation exposure, has long been observed to correlate with skin color. Dark-skinned individuals typically tolerate longer sun exposure compared to light-skinned individuals before experiencing sunburn reactions. In clinical practice, MED and MMD are commonly used to measure the sensitivity of different skin types to UV induced erythema and pigmentation, respectively [RPW10]. Therefore, to more accurately showcase the appearance variation of different skin tones under UV radiation exposure, we first need to calculate the MED and MMD for various skin tones.

Early research aims to establish the Fitzpatrick skin phototype (SPT) classification [Fit88] to calculate MED and MMD, which is based on sun reactiveness [KPCMC*22, OHLK21]. Recently, more objective classification systems have been developed to represent skin color in CIE Lab color space coordinates. Based on reflectance colorimeter, the individual typology angle (ITA) [CCH91] measures skin's constitutive pigmentations to calculate the level of adaptation to UV radiation exposure. After converting the skin color from RGB space to CIE Lab coordinates, ITA is calculated as:

$$\text{ITA} = \arctan[(L^* - 50)/b^*] \times 180/\pi \quad (1)$$

where L* represents luminance ranging from black (0) to white (100) and b* ranges from yellow to blue. The differences along the luminance axis and along the yellowblue axis determine the intensity of skin pigmentation. In general, the higher ITA, the lighter the skin.

In addition, Cole [Col20] has tried to establish the relationship

between an individual's skin color, reflected by their ITA, and their sensitivity to burn from UV radiation, represented by MED:

$$\text{MED} = \text{ITA}^2 \times 0.051 - \text{ITA} \times 10.718 + 629.32. \quad (2)$$

Accordingly, MMD can be inferred due to the relationship between MED and MMD [SIO*85]:

$$\text{MMD} = 0.84 + 1.31\text{MED}. \quad (3)$$

3.2. Erythema Mechanism

Erythema has been seen as one of the most visible skin responses to excessive UV radiation exposure. To quantitatively assess the erythema phenomenon after UV irradiation, our erythema mechanism consists of two parts [Dif21]: peak erythema and erythema time-course calculations. Firstly, as the skin is exposed to increasing doses of UV radiation, there is no observable response until the input UV dose reaches MED. With continued dose escalation, erythema intensity increases, although the rate of increase diminishes at higher doses. Eventually, even with high doses, redness reaches a plateau due to maximal vasodilation having been achieved. Secondly, the time course of UV induced erythema after a single exposure exhibits a rapid onset, followed by a gradual decline. Figure 3 shows the duration of redness, which varies depending on the exposure dose and the extent of maximal erythema.
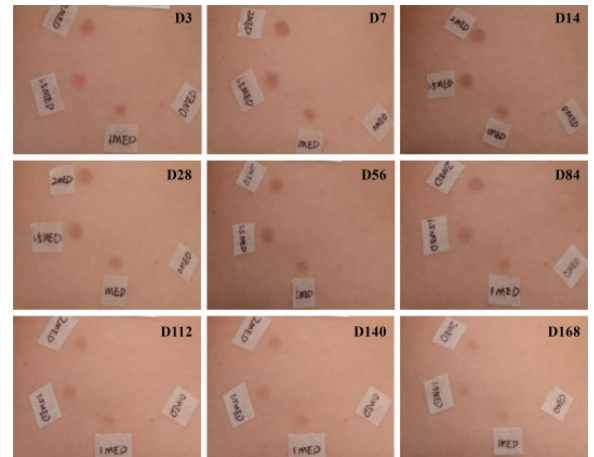

Figure 3: *A depiction of the temporal evolution of skin color alterations resulting from varying doses of solar-simulated UV irradiation, based on sequential photographs captured from a single participant [WHX*17].*

According to experimental research, for UV sources like sunlight, the MED is apparent at about 15% of maximal redness, and 6-10 MED corresponds to maximal redness [DF17]. As shown in Figure 4, the sigmoid function is chosen to describe the degree of erythema, relative to maximal erythema [Dif21]. We use this function to define the fraction of maximal skin redness f due to a UV dose input ψ:

$$f(\psi) = (1 + \alpha(\frac{\psi}{\text{MED}})^{-\beta})^{-1} \quad (4)$$
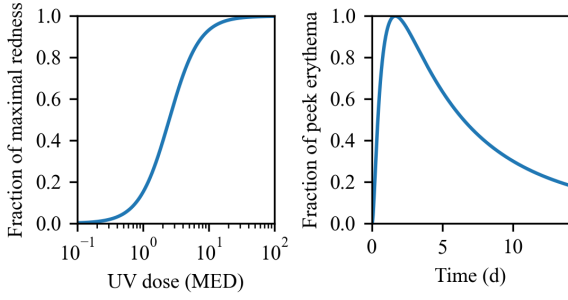
Figure 4: *Left: The erythema response-UV dose curve illustrates the nature of the skin's reaction to UV radiation exposure. Erythema is described qualitatively, starting with no visible redness at doses below 1 MED and intensifying from pale pink to deep red as the severity of erythema increases from minimal to mild, moderate, and then marked. Right: The time course of erythema is depicted relative to the peak redness following a single UV radiation exposure.*

where $\alpha = 1/0.15 - 1$ and $\beta = \ln\frac{1/0.15-1}{1/0.9-1}/\ln(8)$ meaning that the UV doses of 1 MED and 8 MED result in 15% and 90% of maximal redness respectively.

Following a single exposure, the time course of erythema shows a rapid rise peaking at about 40 hours after irradiation, and then a slow disappearance. This time profile is shown in Figure 4, and the erythema relative to the maximum redness, $R(t)$, at time Δt following exposure can be expressed as:

$$R(\Delta t) = \exp(-\frac{(\ln(\Delta t) - \mu)^2}{\theta}) \quad (5)$$

where μ is the natural logarithm of the time after exposure that erythema peaks. θ is expressed as $(\ln(T_{half}) - \mu)^2/\ln(2)$, where T_{half} is the time at which erythema falls to 50% of the peak value.

Considering the maximal vasodilation, we define k_v as how large blood vessels can expand. Therefore, the maximal blood concentration is described as:

$$c_{max} = k_v c_{base} \quad (6)$$

where c_{base} is the initial blood concentration.

We assume that the degree of vasodilation is positively correlated with the degree of erythema. Thus, we define the maximal variation of blood concentration over time $\Delta c'(\psi_i)$ caused by each UV irradiation ψ_i:

$$\Delta c'(\psi_i) = f(\psi_i)(c_{max} - c_{base}) \quad (7)$$

Then, we obtain the variation of blood concentration $\Delta c(t, t_i, \psi_i)$ at time t resulting from UV irradiation at time t_i by multiplying the maximal variation of blood concentration over time and the time course of erythema:

$$\Delta c(t, t_i, \psi_i) = R(t - t_i)\Delta c'(\psi_i) \quad (8)$$

Eventually, we can easily get the blood concentration $c(t)$ at time t from the sum of variations of blood concentration. Notably, we need to clamp the sum with the maximal blood concentration because of the maximal vasodilation:

$$c(t) = \min(\sum_i^n \Delta c(t, t_i, \psi_i), c_{max}) \quad (9)$$

where n is the number of UV doses. The change of blood concentration results in the change of the absorption coefficient of dermis media, and changes the redness of the skin appearance.

3.3. Tanning Mechanism

Our tanning mechanism refers to the work proposed by Chen et al. [CB19]. According to Figure 5, the melanin distribution in the main epidermal layers occurs through two processes: direct production within each layer by melanocytes via melanogenesis, and transfer from the layer below through cell migration. Conversely, melanin can be removed from each layer through natural degradation or upward transfer to the layer above.
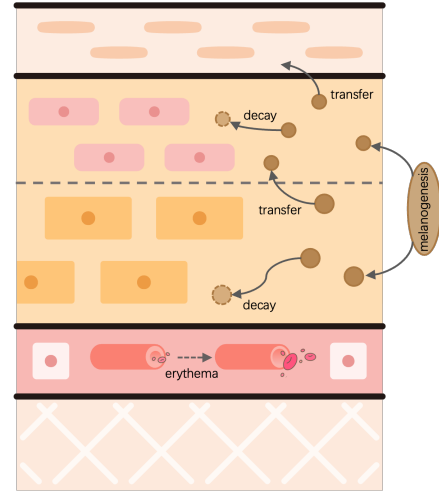

Figure 5: *Schematic representation of the erythema and tanning phenomena considered in the dynamic simulation.*

For clarity, the melanin content within a layer is denoted as m, while the relative proportion of melanin within a specific epidermal layer compared to the total melanin content across all layers is expressed as $\hat{m}$.

The rate of melanin production in a specific layer at time t, denoted by i (where $i = 1, 2, 3$), is represented as $m_{p,i}(t)$ and the fraction of melanin transferred from layer i to the layer above is denoted as $m_{t,i}(t)$. The relative melanin content in layer i is expressed as:

$$\hat{m}_i(t) = m_{p,i}(t) + \delta_m(1 - m_{t,i}(t - \Delta t))\hat{m}_i(t - \Delta t) \\ + m_{t,i}(t - \Delta t)\hat{m}_{i-1}(t - \Delta t) \quad (10)$$

where δ_m represents the fraction of melanin that remains after melanin degradation and Δt means the time interval from the last sampling.

Finally, for each layer i at time t, the updated melanin content

can be calculated by:

$$m_i(t) = \frac{\hat{m}_i(t)}{\tau_i} \sum_{\tau=1}^{3} (\bar{m}_i \tau_i) \tag{11}$$

where $\bar{m}_i$ is the original melanin content for layer i and τ_i corresponds to the original thickness of layer. The change of melanin concentration results in the change of the absorption coefficient of epidermis media, and changes the darkness of the skin appearance.

Analyzed in [LBMZ04, PGM87], the thickness of epidermis is subjected to change during tanning mechanism. The control of skin thickness results from two opposing processes: cell generation and loss. The production rate of skin cells, represented by $\tau_p(t)$, can be expressed as:

$$\tau_p(t) = M'(t)\tau_{p,tan} + \tau_{p,base} \tag{12}$$

In Equation 12, $\tau_{p,base}$ denotes the baseline rate of skin cell production, $\tau_{p,tan}$ represents the increase in this production rate, and $M'(t)$ acts as a modifier influencing this augmentation. The actual skin thickness is then given:

$$\tau(t) = \tau_p(t) + \tau(t - \Delta t))\delta_\tau \tag{13}$$

where $\delta_\tau \in [0,1]$ accounts for the loss in skin cells. The change of thickness of epidermis affects the possibility of light absorption and scattering in epidermis media, and changes the skin appearance.

3.4. Biophysically-based Skin Model

Any skin rendering model using biophysical parameters as inputs can be integrated with our mechanisms. For this work, we refer to a state-of-art biophysically-based skin model proposed by Chen et al. [CBKM15] to build a skin model which is easy to implement. The skin model has thirteen layers, consisting of seven BSDFs (bidirectional scattering distribution function) and six medium layers. Each layer is considered as a semi-infinite plane.

Each medium layer can be regard as a homogeneous medium. To obtain the attenuation coefficient σ_t of each medium layer, we observe the iteration of the model proposed by Chen et al. [CBKM15]. In fact, the process that their model generates distances is equivalent to generating a sample along current majorant segment in volume rendering. This means that every spectral attenuation coefficient $\mu(\lambda)$ of a tissue corresponds to an absorption coefficient $\sigma_a(\lambda)$ or a scattering coefficient $\sigma_s(\lambda)$. Actually, the spectral attenuation coefficient of an absorber is the same as an absorption coefficient, and the spectral attenuation coefficient of an attenuator is the same as an scattering coefficient. Besides, the attenuation coefficient, the sum of the absorption coefficient and the scattering coefficient ($\sigma_t(\lambda) = \sigma_a(\lambda) + \sigma_s(\lambda)$), corresponds to the selection of the smallest of generated distances. Note that if a medium layer does not contain any attenuator, $\sigma_s(\lambda)$ is zero. Take the papillary dermis layer as an example. We denote oxyhemoglobin, deoxyhemoglobin, carboxyhemoglobin, methemeglobin, sulfhemoglobin, beta-carotene and bilirubin by *oh*, *dh*, *ch*, *mh*, *sh*, *bc*, *bil* respec-

tively. The absorption coefficient is described as:

$$\begin{aligned}
\sigma_a^p(\lambda) = &\zeta_{water}(\lambda)c_{water}^p + \zeta_{lipids}(\lambda)c_{lipids}^p \\
&+ (\zeta_{oh}(\lambda)c_{oh}^b + \zeta_{dh}(\lambda)c_{dh}^b + \zeta_{ch}(\lambda)c_{ch}^b \\
&+ \zeta_{mh}(\lambda)c_{mh}^b + \zeta_{sh}(\lambda)c_{sh}^b + \zeta_{bc}(\lambda)c_{bc}^b \\
&+ \zeta_{bil}(\lambda)c_{bil}^b)c_{blood}^p
\end{aligned} \tag{14}$$

where ζ_k, c_k^p and c_k^b mean respectively to the specific absorption coefficient of a biological substance k, its concentration within the papillary dermis and its concentration within whole blood. The scattering coefficient is described as:

$$\sigma_s^p(\lambda) = \frac{128\pi^5 r^6 c_f}{3\lambda^4} \left(\frac{4}{3}\pi r^3\right)^{-1} \left(\frac{\eta^2 - 1}{\eta^2 + 1}\right)^2 \tag{15}$$

where r, c_f and η correspond to the radius of connective fibers, the concentration of connective fibers and the ratio between the refractive index of connective fibers to the surrounding medium one.

The phase function of each medium layer is determined by the scattering process of attenuators. We use Rayleigh phase function [Can78] to replace the scattering process arising from connective fibers. Therefore, the phase function of the papillary dermis can be calculated by:

$$p(\cos\theta) = \frac{3}{4}(1 + \cos^2(\theta)) \tag{16}$$

where θ is the polar angle of the perturbed ray. Due to the fact that the particle nature of melanosomes affects little in the visible region [Che16], we remove the implementation of melanosomes and move their contents to melanin for simplicity.

3.5. Rendering Pipeline

The rendering pipeline is described in a part of Figure 2. Our skin appearance model can be implemented by using volumetric path tracing as integrating method. We take one layer of our model as an example.

When a ray comes from the upper layer including skin outside, it firstly intersects with the Trowbridge-Reitz BSDF or Fresnel BSDF upon the medium. The BSDF handles the intersecting ray from the upper layer or the medium underlying it, and determines whether the ray is reflected or refracted. If the ray is reflected from the upper layer or refracted from the medium, it advances to the upper layer. If the ray is refracted from the upper layer or reflected from the medium, it advances to intersect with the medium.

The homogeneous medium handles rays from the BSDF upon it and the lower layer. When a ray goes through the medium, it is commonly handled the following way in volumetric path tracing. Firstly, we check the intersection between the ray and the bounding box of the medium. If there is any intersection, we then sample a distance along the ray. Finally, we retrieve the medium scattering coefficient and the phase function for this sampled position and modify the weight and direction of the ray. Once the direction of the ray leaving the medium is determined, we check which part of our model the ray goes next. If the direction of the ray is upward, it intersects the BSDF upon the medium. If the direction of the ray is

horizontal, it is terminated because it no longer intersects any part. If the direction of the ray is downward, it intersects the lower layer.

The ray continues the loop mentioned above until it leaves the skin. Note that the lowest layer consists of only a diffuse BSDF, which means that it just reflects all the rays.

Algorithm 1 describes how a ray travels through an interface and a medium layer in a pseudo-code form. The incoming position *pos* is later used to BSSRDF sampling [KKCF13] to achieve the translucency effect.

4. Experimental Results

Our method is implemented within PBRT-V4 [PJH23] integrated with GPU rendering. We use time-steps of 1 hour in our simulation mechanism. All skin datasets used in experiments can be checked in Appendix A. Our results show high quality renderings at a low time cost. It takes about 6 minutes to render a image with 500 pixels height, 500 pixels width and 32768 samples per pixel on an NVIDIA GeForce RTX 4070 GPU in the following experiments.

4.1. Quantitative Comparisons

We compare the predictions of our simulation method with the results of controlled experiments performed by Masuda et al. [MYHT09].

Firstly, we calculate the MED and MMD of dataset I using ITA described in Section 3.1. We put a skin sample in an infinity white light source environment. By adjusting the intensity of the light source, we get an acceptable skin color which is then converted to ITA to obtain the MED and MMD results (MED = 1.729, MMD = 2.274).

Then we use the calculated MED and MMD to compare the skin appearance changes conducted by 1.75 MED in L*a*b* color space. As it can be observed in Figure 6, both the lightness (L*) and redness (a*) coordinates show good agreement.

We proceed to employ the same UV radiation exposure dose schedule to our skin model to see the rendering results. In Figure 7, we can see that the exposed skin gets redder first, and then gets blacker gradually, which is consistent with the actual behavior of skin after sunlight exposure.

4.2. Comparisons with Previous Works

We also compare our simulation with previous works by Chen et al. [CB19]. We conduct the same UV radiation exposure dose schedule (10 SED, 1 SED = 100 J/m^2) on both our simulation and simulation by Chen et al. [CB19] using dataset II, shown in Figure 8. Similar to Section 4.1, we obtain the MED and MMD of dataset II at first: $MED_{II} = 1.465$, $MMD_{II} = 1.928$. Apparently, Chen's simulation does not show the trend of turning red, while our simulation shows the characteristics of erythema, especially in the first day and the second day.

Algorithm 1: Sampling for an interface and a medium layer.

Input: The outgoing direction ω_o.
Output: The incoming direction ω_i, BRDF value f, probability p and incoming position pos.

```
1   pos ← (0,0)
    // Handle the interaction with the interface
2   Sample the interface with ωₒ and get ωᵢ, f, p
3   if the interface reflects ωₒ then
4   │   return ωᵢ, f, p, pos
5   end
    // Handle interactions with the medium
6   f ← f|ωᵢ.z|
7   z ← thickness
8   for depth ← 1 to maxDepth do
9   │   if ωᵢ.z = 0 then
10  │   │   return Bad sample
11  │   end
12  │   Get medium coefficient σₐ, σₛ and σₜ
13  │   Sample a depth distance dz from p(x) = σₜ/|ωᵢ.z| e^(−σₜ/|ωᵢ.z| x)
14  │   if ωᵢ.z > 0 then
15  │   │   z ← z + dz
16  │   else
17  │   │   z ← z − dz
18  │   end
19  │   if 0 < z < thickness then
20  │   │   Update f and pos with the distance dz
21  │   │   Sample whether the ray is absorbed or scattered
22  │   │   if the ray is absorbed then
23  │   │   │   return Bad sample
24  │   │   else
25  │   │   │   Update f for the scattering decision
26  │   │   │   Sample the phase function and update ωᵢ, f, p
27  │   │   │   continue
28  │   │   end
29  │   else
30  │   │   Update f and pos with the distance from the
        │   │   previous position to the medium boundary which
        │   │   the ray hits
31  │   │   Update z to the medium boundary which the ray hits
32  │   end
33  │   if z=0 then
        │   // The ray goes down
34  │   │   Sample the lower layer and update ωᵢ, f, p, pos
35  │   else
        │   // The ray goes up
36  │   │   Sample the interface and update ωᵢ, f, p
37  │   │   if the interface refracts ωᵢ then
38  │   │   │   return ωᵢ, f, p, pos
39  │   │   end
40  │   end
41  │   f ← f|ωᵢ.z|
42  end
43  return Bad sample
```

Xueyan He et al. / Biophysically-based Simulation of Sun-induced Skin Appearance Changes
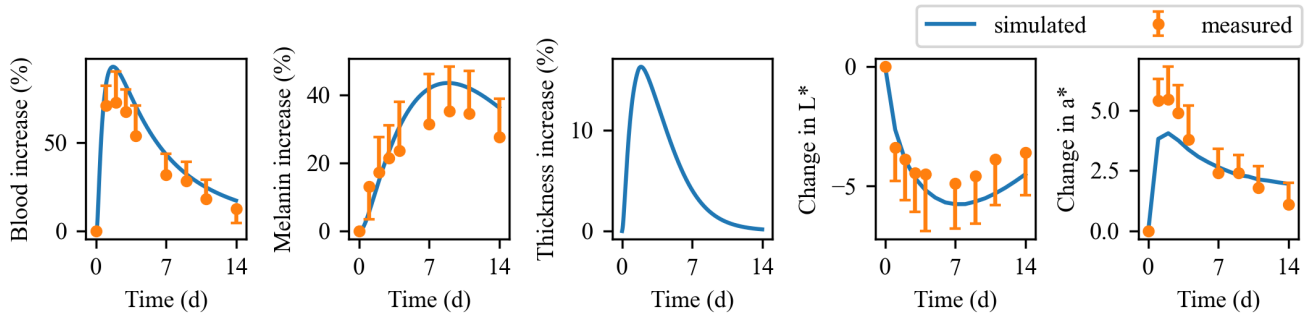

Figure 6: *We conduct the same UV radiation exposure dose schedule (1.75 MED) as experiments performed by Masuda et al. [MYHT09] on our simulation model. From left to right: the increase of blood in dermis, the increase of melanin in epidermis, the increase of thickness of epidermis, the appearance change of skin in lightness, the appearance change of skin in redness. The blue curves are our simulation results, while the orange points are the actual results. Note that Masuda et al. [MYHT09] do not measure the change of thickness of epidermis, so there is no measured points in the third plot.*

Figure 7: *Sequence of images illustrating appearance changes on skin over a period of 15 days due to the UV radiation exposure schedule described in Section 4.1. The number of the day increases by one from left to right, top to bottom. The image on the upper left corner shows initial status (Day 0). The exposure area is bounded because of the vest wearing.*
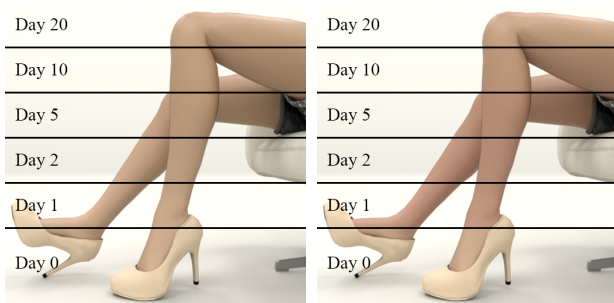
Figure 8: *Comparisons with previous work. The left image is performed by simulation by Chen et al. [CB19]. The right image is performed by our simulation. The number of day increases from bottom to top.*

4.3. Comparisons with Different Dose Schedules

Figure 9 shows how skin appearance changes when it is induced by different UV radiation exposure dose schedules. It can be seen that effect of turning red and black is more obvious with a larger dose schedule. Besides, it takes a longer time for the skin to return the initial status when it is induced by a larger dose schedule.

4.4. Comparisons with Different Types of Skin

We proceed to employ the same UV dose schedule (10 SED) on dataset II, III and IV to see the different trends of skin appearance changes. We obtain the MEDs and MMDs of dataset III and IV: $MED_{III} = 1.986$, $MMD_{III} = 2.610$, $MED_{IV} = 4.385$, $MMD_{IV} = 5.752$. The result of MEDs and MMDs accords with the actual result that darker people have larger MED and MMD.

After we get MEDs and MMDs of three datasets, we expose a part of an arm, a smiley face, to irradiation, shown in Figure 10. As we can see, the darker skin has a smaller trend to become redder and darker. One reason is that the darker skin has larger MED and MMD, which means that the fraction of UV dose and MED or MMD is smaller, leading to a smaller change in skin material concentrations. Another reason is that the darker skin has higher melanin and blood concentrations, resulting in a smaller skin appearance change even though their concentrations change.

5. Conclusion

In this paper, we propose a discrete time-stepping mechanism to describe the temporal influence of UV radiation on skin appearance. This model enables the simulation of erythema and tanning effects under specific UV doses over time, facilitating precise assessment of skin reactions across various skin tones. In terms of skin structure simulation, our method incorporates seven BSDFs and six homogeneous medium layers, providing a comprehensive representation of skin properties. Through spectral analysis, our model accurately calculates absorption and scattering coefficients for each layer, considering various biological substances and their concentrations.

Additionally, we develop a rendering pipeline that showcases the appearance variations of different skin tones under UV radiation. Implemented using volumetric path tracing, the pipeline offers a comprehensive approach to simulating light interaction within skin layers. It efficiently handles ray intersections with Trowbridge-Reitz or Fresnel BSDFs, accurately modeling reflection and refraction behaviors. Additionally, the inclusion of a homogeneous medium ensures realistic light scattering and absorption within the skin, enhancing the overall visual fidelity. By seamlessly integrating these components, our method delivers nuanced and physically plausible rendering results, capturing the intricate details of skin appearance with precision.

References

[AF21]   ABDLATY R., FANG Q.: Skin erythema assessment techniques. *Clinics in Dermatology 39*, 4 (2021), 591–604. Diagnostic and therapeutic instrumentation in dermatology. `doi:10.1016/j.clindermatol.2021.03.006`. 3

[BGZ01]   BENRATH J., GILLARDON F., ZIMMERMANN M.: Differential time courses of skin blood flow and hyperalgesia in the human sunburn reaction following ultraviolet irradiation of the skin. *European Journal of Pain 5*, 2 (2001), 155–167. `doi:10.1053/eujp.2001.0229`. 3

[Can78]   CANTOR A.: Optics of the atmosphere–scattering by molecules and particles. *IEEE Journal of Quantum Electronics 14*, 9 (1978), 698–699. `doi:10.1109/JQE.1978.1069864`. 6

[CB19]   CHEN T. F., BARANOSKI G. V. G.: A physiologically-based framework for the simulation of skin tanning dynamics. In *Dynamics and Fluctuations in Biomedical Photonics XVI* (2019), Tuchin V. V., Leahy M. J., Wang R. K., (Eds.), vol. 10877, International Society for Optics and Photonics, SPIE, p. 108770H. `doi:10.1117/12.2504672`. 1, 2, 3, 5, 7, 9, 12

[CBKM15]   CHEN T. F., BARANOSKI G. V. G., KIMMEL B. W., MIRANDA E.: Hyperspectral modeling of skin appearance. *ACM Trans. Graph. 34*, 3 (may 2015). `doi:10.1145/2701416`. 2, 4, 6, 12

[CCH91]   CHARDON A., CRETOIS I., HOURSEAU C.: Skin colour typology and suntanning pathways. *International Journal of Cosmetic Science 13*, 4 (1991), 191–208. `doi:10.1111/j.1467-2494.1991.tb00561.x`. 4

[Che16]   CHEN T. F.: *On the Modelling of Hyperspectral Light and Skin Interactions and the Simulation of Skin Appearance Changes Due to Tanning*. PhD thesis, 2016. URL: `http://hdl.handle.net/10012/10105`. 6

[Chr15]   CHRISTENSEN P. H.: An approximate reflectance profile for efficient subsurface scattering. In *ACM SIGGRAPH 2015 Talks* (New York, NY, USA, 2015), SIGGRAPH '15, Association for Computing Machinery. `doi:10.1145/2775280.2792555`. 2

[CKB16]   CHIANG M. J.-Y., KUTZ P., BURLEY B.: Practical and controllable subsurface scattering for production path tracing. In *ACM SIGGRAPH 2016 Talks* (New York, NY, USA, 2016), SIGGRAPH '16, Association for Computing Machinery. `doi:10.1145/2897839.2927433`. 2

[Col20]   COLE C.: Global data of unprotected skin minimal erythema dose relationship to individual typology angle. *Photodermatology, Photoimmunology & Photomedicine 36*, 6 (2020), 452–459. `doi:10.1111/phpp.12592`. 4

[DF17]   DIFFEY B., FARR P.: Ultraviolet erythema: dose response and mediator diffusion. *Photochem. Photobiol. Sci. 17* (10 2017). `doi:10.1039/C7PP00228A`. 2, 4

[Dif21]   DIFFEY B.: Erythema and acclimatization following repeated sun exposure: A modeling study. *Photochemistry and Photobiology 97*, 6 (2021), 1558–1567. `doi:10.1111/php.13466`. 2, 3, 4

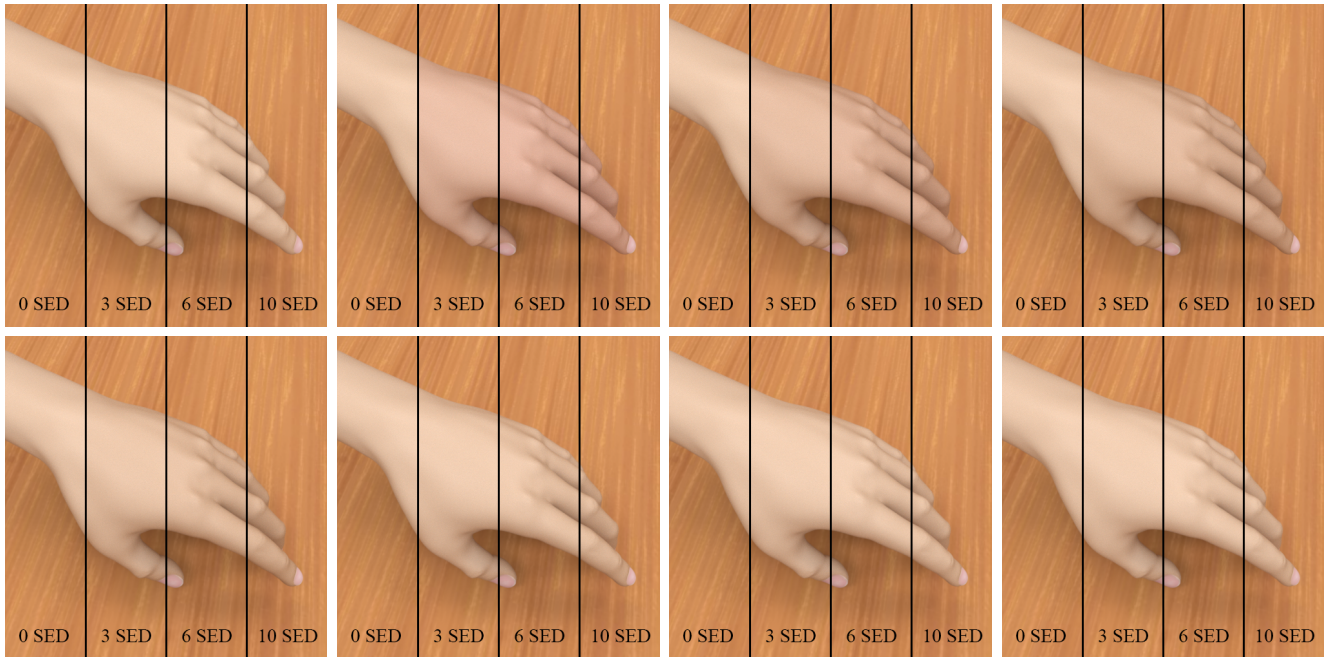[DJ05]   DONNER C., JENSEN H. W.: Light diffusion in multi-layered

Figure 9: *Comparisons with different dose schedules. Each image splits into four parts. Dose increases from 0 SED to 10 SED from left to right in each image. The number of day increases from left to right, top to bottom (Day 0, 2, 6, 10, 20, 30, 40, 50).*

translucent materials. *ACM Trans. Graph. 24*, 3 (jul 2005), 10321039. doi:10.1145/1073204.1073308. 2

[DJ06] DONNER C., JENSEN H. W.: A Spectral BSSRDF for Shading Human Skin. In *Symposium on Rendering* (2006), Akenine-Moeller T., Heidrich W., (Eds.), The Eurographics Association. doi:/10.2312/EGWR/EGSR06/409-417. 2

[EKPR20] EGAMBARAM O. P., KESAVAN PILLAI S., RAY S. S.: Materials science challenges in skin uv protection: A review. *Photochemistry and Photobiology 96*, 4 (2020), 779–797. doi:10.1111/php.13208. 1

[Fit88] FITZPATRICK T. B.: The Validity and Practicality of Sun-Reactive Skin Types I Through VI. *Archives of Dermatology 124*, 6 (06 1988), 869–871. doi:10.1001/archderm.1988.01670060015008. 4

[Han15] HANIKA JOHANNESÄAND DROSKE M. F. L.: Manifold Next Event Estimation. *Computer Graphics Forum* (2015). doi:10.1111/cgf.12681. 2

[IGAJG15] IGLESIAS GUITIÁN J., ALIAGA C., JARABO A., GUTIÉRREZ D.: A biophysically-based model of the optical properties of skin aging. *Computer Graphics Forum 34* (05 2015), 45–55. doi:10.1111/cgf.12540. 1, 2

[JB02] JENSEN H. W., BUHLER J.: A rapid hierarchical rendering technique for translucent materials. *ACM Trans. Graph. 21*, 3 (jul 2002), 576581. doi:10.1145/566654.566619. 2

[Jim12] JIMENEZ J.: Separable subsurface scattering. In *ACM SIGGRAPH 2012 Computer Animation Festival* (New York, NY, USA, 2012), SIGGRAPH '12, Association for Computing Machinery, p. 82. doi:10.1145/2341836.2341906. 2

[JKLY23] JUNG G., KIM S., LEE J., YOO S.: Deep learning-based optical approach for skin analysis of melanin and hemoglobin distribution. *Journal of Biomedical Optics 28* (03 2023). doi:10.1117/1.JBO.28.3.035001. 2

[JSB*10] JIMENEZ J., SCULLY T., BARBOSA N., DONNER C., AL-

VAREZ X., VIEIRA T., MATTS P., ORVALHO V., GUTIÉRREZ D., WEYRICH T.: A practical appearance model for dynamic facial color. *ACM Trans. Graph. 29* (12 2010), 141. doi:10.1145/1866158.1866167. 2

[KB04] KRISHNASWAMY A., BARANOSKI G. V.: A biophysically-based spectral model of light interaction with human skin. *Computer Graphics Forum 23*, 3 (2004), 331–340. doi:10.1111/j.1467-8659.2004.00764.x. 2

[KKCF13] KING A., KULLA C., CONTY A., FAJARDO M.: Bssrdf importance sampling. In *ACM SIGGRAPH 2013 Talks* (New York, NY, USA, 2013), SIGGRAPH '13, Association for Computing Machinery. doi:10.1145/2504459.2504520. 7

[KNK*16] KOERNER D., NOVAK J., KUTZ P., HABEL R., JAROSZ W.: Subdivision Next-Event Estimation for Path-Traced Subsurface Scattering. In *Eurographics Symposium on Rendering - Experimental Ideas & Implementations* (2016), Eisemann E., Fiume E., (Eds.), The Eurographics Association. doi:10.2312/sre.20161214. 2

[KPCMC*22] KRUTMANN J., PIQUERO-CASALS J., MORGADO-CARRASCO D., GRANGER C., TRULLAS C., PASSERON T., LIM H.: Photoprotection for people with skin of colour: needs and strategies. *British Journal of Dermatology 188* (11 2022). doi:10.1093/bjd/ljac046. 4

[LATdO*97] LOCK-ANDERSEN J., THERKILDSEN P., DE OLIVARIUS F. F., GNIADECKA M., DAHLSTREM K., POULSEN T., WULF H.-C.: Epidermal thickness, skin pigmentation and constitutive photosensitivity. *Photodermatology, Photoimmunology & Photomedicine 13*, 4 (1997), 153–158. doi:10.1111/j.1600-0781.1997.tb00220.x. 3

[LBMZ04] LOPEZ H., BEER J. Z., MILLER S. A., ZMUDZKA B. Z.: Ultrasound measurements of skin thickness after uv exposure: a feasibility study. *Journal of Photochemistry and Photobiology B: Biology 73*, 3 (2004), 123–132. doi:10.1016/j.jphotobiol.2003.11.004. 3, 6

[MYHT09] MASUDA Y., YAMASHITA T., HIRAO T., TAKAHASHI M.: An innovative method to measure skin pigmentation. *Skin Research and*

Figure 10: *Comparisons with different types of skin. Images on the first, second, third rows use dataset II, III and IV in sequence. The number of day increases from left to right (Day 0, 2, 6, 10). Images on the first column shows the initial status of the skin. The exposed area on the arm is a smile face.*

Technology 15, 2 (2009), 224–229. doi:10.1111/j.1600-0846.2009.00359.x. 7, 8

[OHLK21] OSTO M., HAMZAVI I., LIM H., KOHLI I.: Individual typology angle and fitzpatrick skin phototypes are not equivalent in photodermatology. *Photochemistry and Photobiology 98* (11 2021). doi:10.1111/php.13562. 4

[PGM87] PEARSE A. D., GASKELL S. A., MARKS R.: Epidermal changes in human skin following irradiation with either uvb or uva. *Journal of Investigative Dermatology 88*, 1 (1987), 83–87. doi:https://doi.org/10.1111/1523-1747.ep12465094. 6

[PJH23] PHARR M., JAKOB W., HUMPHREYS G.: *Physically based rendering: from theory to implementation*, fourth edition. ed. The MIT Press, Cambridge, Massachusetts, 2023. 7

[RPW10] RAVNBAK M., PHILIPSEN P., WULF H.: The minimal melanogenesis dose/minimal erythema dose ratio declines with increasing skin pigmentation using solar simulator and narrowband ultraviolet b exposure. *Photodermatology, photoimmunology photomedicine 26* (06 2010), 133–7. doi:10.1111/j.1600-0781.2010.00508.x. 2, 4

[SIO*85] SHONO S., IMURA M., OTA M., ONO S., TODA K.: The

relationship of skin color, uvb-induced erythema, and melanogenesis. *Journal of Investigative Dermatology 84*, 4 (1985), 265–267. doi:10.1111/1523-1747.ep12265342. 4

[SK04] STAMATAS G., KOLLIAS N.: Stamatas gn, kollias nblood stasis contributions to the perception of skin pigmentation. j biomed opt 9:315-322. *Journal of biomedical optics 9* (03 2004), 315–22. doi:10.1117/1.1647545. 3

[SLDW22] SCHMALWIESER A., LOHR M., DALY S., WILLIAMS J.: Modeling acute and cumulative erythemal sun exposure on vulnerable body sites during beach vacations utilizing behavior-encoded 3d body models. *Photochemical Photobiological Sciences 22* (08 2022). doi:10.1007/s43630-022-00293-1. 1, 2

[WHX*17] WAN M., HU R., XIE X., GONG Z., YI J., CHEN H., XIE L., GUAN X., GUAN L., LAI W.: Skin erythema, pigmentation and hydration kinetics after ultraviolet radiation-induced photodamage in southern chinese women. *Photochemistry and Photobiology 93*, 5 (2017), 1276–1281. doi:10.1111/php.12752. 4

[WVH17] WRENNINGE M., VILLEMIN R., HERY C.: Path traced subsurface scattering using anisotropic phase functions and non-exponential

free flights. URL: https://api.semanticscholar.org/CorpusID:37696320. 2

Appendix A: Skin Datasets

Datasets for our skin model is shown on Table 5. Table 2 and Table 3 are for melanin mechanism. All of them are extracted from datasets by Chen et al. [CBKM15, CB19]. And Table 4 is used for erythema mechanism.

Parameter	Value
Stratum Granulosum $m_{p,i,c}$	0
Stratum Granulosum $m_{t,i,c}$	0.0004
Stratum Granulosum $m_{p,i,f}$	0
Stratum Granulosum $m_{t,i,f}$	0
Stratum Spinosum $m_{p,i,c}$	0
Stratum Spinosum $m_{t,i,c}$	0.0051
Stratum Spinosum $m_{p,i,f}$	0
Stratum Spinosum $m_{t,i,f}$	0.02
Stratum Basale $m_{p,i,c}$	0.01
Stratum Basale $m_{t,i,c}$	0.0081
Stratum Basale $m_{p,i,f}$	0.011
Stratum Basale $m_{t,i,f}$	0.045
δ_{e_o}	0.98
δ_{s_o}	0.99
δ_s	0.985
δ_m	0.99
κ	0.7
ω	500

Table 2: *Dataset for melanin simulation.*

Parameter	Value
$\delta_{e_o'}$	0.985
$\delta_{s_o'}$	0.2
$\delta_{s'}$	0.98
δ_τ	0.9
κ'	1
ω'	20
$\tau_{p,base}$	0.1
$\tau_{p,tan}$	0.025

Table 3: *Dataset for thickness simulation.*

Parameter	Value
α	5.667
β	1.891
μ	3.689
T_{half}	156
k_v	3.5

Table 4: *Dataset for erythema simulation.*

Parameter	I	II	III	IV
Surface Fold Aspect Ratio	0.15	0.25	0.25	0.45
Stratum Corneum Thickness (cm)	0.001	0.001	0.001	0.0002
Stratum Granulosum Thickness (cm)	0.0017	0.0017	0.0033	0.0007
Stratum Spinosum Thickness (cm)	0.0017	0.0017	0.0033	0.0007
Stratum Basale Thickness (cm)	0.0017	0.0017	0.0033	0.0007
Papillary Dermis Thickness (cm)	0.02	0.02	0.01	0.023
Reticular Dermis Thickness (cm)	0.1	0.1	0.1	0.2
Stratum Granulosum Melanin Content (%)	1.8	1.8	1.25	25
Stratum Spinosum Melanin Content (%)	1.8	1.8	1.25	25
Stratum Basale Melanin Content (%)	1.8	1.8	5	25
Melanosome Eumelanin Concentration (mg/mL)	90	50	50	50
Melanosome Pheomelanin Concentration (mg/mL)	4	4	2	4
Papillary Dermis Blood Content (%)	0.25	0.3	0.2	2.5
Reticular Dermis Blood Content (%)	0.25	0.3	0.2	2.5
Oxygenated Blood Fraction (%)	75	75	95	75
Stratum Corneum Refractive Index	1.55			
Epidermis Refractive Index	1.4			
Papillary Dermis Refractive Index	1.39			
Reticular Dermis Refractive Index	1.41			
Hemoglobin Concentration in Whole Blood (mg/mL)	147			
Methemoglobin Concentration in Whole Blood (mg/mL)	1.5			
Carboxyhemoglobin Concentration in Whole Blood (mg/mL)	1.5			
Sulfhemoglobin Concentration in Whole Blood (mg/mL)	0			
Whole Blood Bilirubin Concentration (mg/mL)	0.003			
Stratum Corneum Beta-carotene Concentration (mg/mL)	2.1e-4			
Epidermis Beta-carotene Concentration (mg/mL)	2.1e-4			
Blood Beta-carotene Concentration (mg/mL)	7.0e-5			
Stratum Corneum Water Content (%)	35			
Epidermis Water Content (%)	60			
Papillary Dermis Water Content (%)	75			
Reticular Dermis Water Content (%)	75			
Stratum Corneum Lipid Content (%)	20			
Epidermis Lipid Content (%)	15.1			
Papillary Dermis Lipid Content (%)	17.33			
Reticular Dermis Lipid Content (%)	17.33			
Stratum Corneum Keratin Content (%)	65			
Stratum Corneum Urocanic Acid Density (mol/L)	0.01			
Skin DNA Density (mg/mL)	0.185			

Table 5: *Skin model datasets.*